Pattern Forming System in the Presence of Different Symmetry-Breaking Mechanisms

G. Seiden,[1] S. Weiss,[1] J. H. McCoy,[2] W. Pesch,[3] and E. Bodenschatz[1,2,4,*]

[1]*Max Planck Institute for Dynamics and Self-Organization, D-37073 Göttingen, Germany*
[2]*Department of Physics, Cornell University, Ithaca, New York 14853-2501, USA*
[3]*Physikalisches Institut, Universität Bayreuth, D-95440 Bayreuth, Germany*
[4]*Institute for Nonlinear Dynamics, Georg August University, D-37077 Göttingen, Germany*

(Received 4 June 2008; published 20 November 2008)

We report experiments on spatially forced inclined layer convection, where the combined effect of the intrinsic symmetry breaking due to a gravity-induced shear flow and spatially periodic 1D forcing is studied. We observed pattern selection processes resulting in stabilization of spatiotemporal chaos and the emergence of novel two-dimensional states. Phase diagrams depicting the different observed states for typical forcing scenarios are presented. Convection in the weakly nonlinear regime is compared with theory, and a good agreement is found.

DOI: 10.1103/PhysRevLett.101.214503 PACS numbers: 47.54.−r, 05.45.−a, 47.52.+j

Understanding pattern formation processes is important in a variety of research areas ranging from economics [1] to neuroscience [2]. Ideally, patterns emerge with a *well-defined* wave vector by a spontaneous symmetry-breaking bifurcation from an initial homogeneous state [3]. Naturally driven systems, however, often contain intrinsic symmetry-breaking elements which influence the observed patterns. This is the case, for example, in atmospheric convection over topography [4] and in fingerprint formation in the presence of normal epidermic displacements [5]. By applying spatially periodic forcing to a carefully controlled pattern forming system, such as Rayleigh-Bénard convection, one is able to get valuable insight into the important role of such symmetry-breaking constituents. It also enables the investigation of pattern-forming aspects that are otherwise difficult to assess, such as the stability regimes of patterns (the "Busse balloon") [6,7], commensurate-incommensurate transitions [8], or defect aggregation resulting in localized coherent states [9]. The combined effect of spatial forcing and other symmetry-breaking mechanisms in a pattern-forming system is largely unexplored [10]. As shown here, inclined layer convection is well suited to study this problem.

Inclined layer convection, in which a thin fluid layer of thickness d is subjected to a temperature gradient $\Delta T/d$ and oriented obliquely with respect to gravity, is a rich variant of isotropic Rayleigh-Bénard convection. The introduction of an in-plane gravitational component through inclination breaks the rotational symmetry. As a result, depending on the inclination angle θ, either longitudinal rolls (buoyancy driven) or transverse rolls (shear-flow driven) set in at onset [11]. The wealth of nonlinear states observed with increasing ΔT has been the focus of recent experimental and theoretical studies [12–14].

In this Letter, we applied periodic forcing at an angle φ with respect to the in-plane gravity component [Fig. 1(a)], with a wave vector $\boldsymbol{q}_f$. By varying θ, we were able to tune the relative importance of the two anisotropies. For a given inclination angle, a 1D roll pattern with a wave vector equal to the forcing wave vector was observed at small ΔT ($\Delta T \ll \Delta T_c$, where ΔT_c is the onset temperature difference of the unforced system). As ΔT was increased, the roll aligning mechanisms due to inclination and forcing started to interact. For $\varphi = 0°$, both mechanisms cooperated and rendered the longitudinal rolls more stable. In particular, undulation chaos [12], which is a state found close to onset for a large range of inclination angles in the unforced system, was strongly suppressed. In contrast, for $\varphi = 90°$, competition and spatial resonances between longitudinal and transverse rolls occurred. This led to qualitatively new patterns, typically with rhombic symmetry, a phenomenon rarely observed in pattern-forming systems.

The experimental system, described in detail in [15], consisted of pressurized CO_2 gas confined in the vertical direction between two parallel, thermally well conducting plates separated by a distance d and held at a desired temperature difference ΔT to within 0.001 °C. Two square convection cells of side lengths $L = 85d$ and $L = 35d$ were used. The side walls were aligned parallel to the inclination direction [y axis in Fig. 1(a)] to avoid undesired, boundary driven, large scale flows. The average temperature used was $T_{\mathrm{av}} = (25.00 \pm 0.02)$ °C, and the pressure in the cell was kept at $P_{\mathrm{av}} = (48.26 \pm 0.03)$ bar throughout the experi-

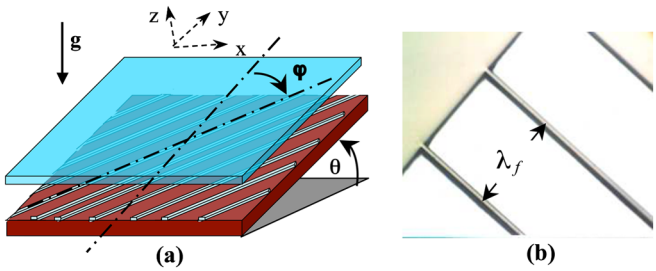

FIG. 1 (color online). (a) Schematic of forced inclined layer convection configuration. (b) Microscope image of fabricated SU-8 stripes on flat plate.

ments. The Prandtl number was $\mathrm{Pr} \equiv \nu/\kappa = 1.3$ (here ν and κ are the kinematic viscosity and thermal diffusivity, respectively). The corresponding Busse parameter was $Q = 0.5$, confirming the validity of the Boussinesq approximation. The patterns were observed by the standard shadowgraph technique [15].

The smaller cell was unforced and served as our reference. For inclination angles below the codimension-two point $\theta_{cd} \cong 80°$, theory predicts a bifurcation at $\Delta T_c(\theta) = \Delta T_c(0)/\cos(\theta)$ to buoyancy driven *longitudinal* rolls. These have a wave number $q_c^L = 3.117/d$ and are aligned with their axes parallel to the inclination direction. Above the codimension-two point, the shear flow driven *transverse* rolls prevail with a wave number $q_c^T \cong 2.81/d$ and aligned with their axis orthogonal to the inclination direction (x axis). The onset of convection in the unforced cell, which has been studied previously [11,12], agreed well with the linear theory [16].

The forcing mechanism in our experiment was surface corrugations, realized by an array of photo-resist (SU-8) stripes fabricated onto the bottom plate [Fig. 1(b)] [9]. The height and width of the stripes were $h = (65 \pm 3)$ μm and $l = (100 \pm 1)$ μm, respectively, and they covered the area of the large square cell with a (1 ± 0.001) mm period, yielding a modulation wave number $q_f = 2\pi/\lambda_f = \pi/0.5$ mm. Keeping only the leading Fourier mode, the surface of the lower plate can thus be described as: $z = -d/2 + z_f$ with $z_f = d[0.1h/d + \delta\cos(q_f x)]$, where the modulation amplitude $\delta = (2/\pi)\sin(\pi/10)h/d$.

Two main cases were investigated. In the first, the forcing SU-8 stripes were aligned parallel to the gravitational component ($\varphi = 0$) and in the second, they were orthogonal ($\varphi = \pi/2$). Phase diagrams for both cases were explored by setting the inclination angle θ and recording the states while slowly scanning the reduced control parameter $\varepsilon = [\Delta T - \Delta T_c(\theta)]/\Delta T_c(\theta)$. The cell height in these experiments was $d = (540 \pm 5)$ μm, resulting in a forcing wave number $q_f = 1.09 q_c^L$. By using long waiting times ($>100\tau_v$, where $\tau_v = d^2/\kappa \sim 3$ s is the vertical thermal diffusion time), care was taken that the system had sufficient time to settle into steady state, before measurements were made.

Parallel forcing.—Figure 2(a) shows the phase diagram for the parallel case. While in the absence of forcing convection sets in via a forward bifurcation at $\varepsilon = 0$, the surface corrugations caused the bifurcation to become imperfect, and we found longitudinal rolls [LR in Fig. 2(b)] even for subcritical values of ΔT (i.e., $-1 < \varepsilon < 0$). For inclination angles $0° \leq \theta < 28°$, the longitudinal roll were stable up to fairly large control parameters ($\varepsilon \sim 1$) before a bifurcation to varicose patterns (VP) was observed. These were spanned by the wave vectors $\mathbf{q_0} = (q_f, 0)$ and $\mathbf{q_1} = s[\cos(\alpha), \sin(\alpha)]$ with $s \cong 0.6 q_f$ and $\alpha \cong 36°$. In the vicinity $\theta \approx 0$, the instability to VP can be interpreted as a finite wave number modification of the well-known modulational ($s \to 0$) skewed-varicose instability of the unforced system for $q > q_c^L$ [17]. The role of transverse modes in the destabilization of forced rolls, which was observed recently also in [9], was not anticipated by theory [18]. For $\theta < 10°$, the VP can coexist with subharmonic resonances (SR) and periodically spaced kink lines (KL). These share some similarity with the 1D soliton states observed in forced electro-hydrodynamic convection with intrinsic anisotropy [8], and explained by theory [18].

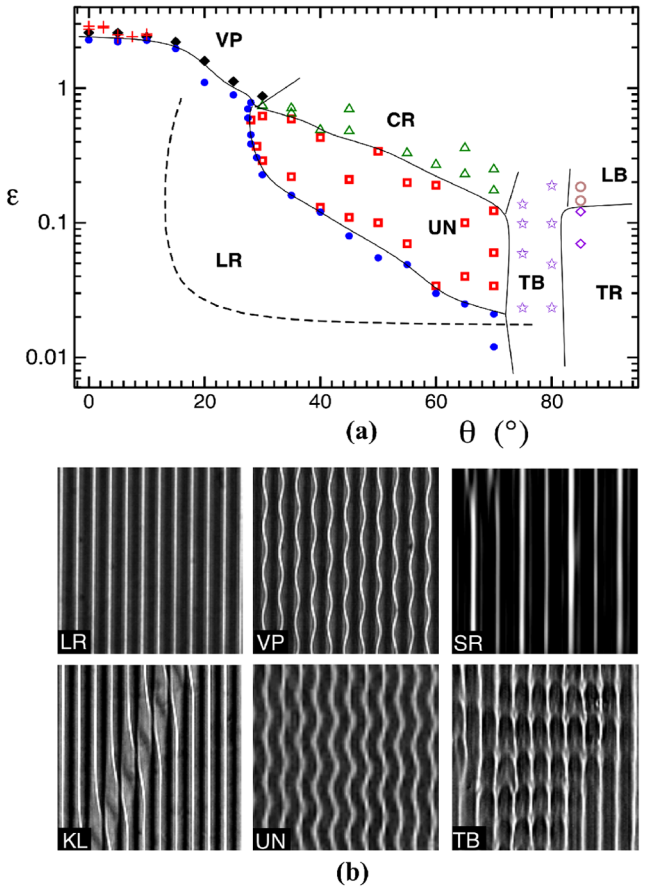

FIG. 2 (color online). Parallel Forcing. (a) Phase diagram. The solid line is a guide to the eye indicating the interface between states. The broken line represents the theoretical curve of the instability to undulation chaos in the unforced case. (b) Selected patterns observed (square area shown has side length equal to $21d$). Upper side of inclined layer is at top part of images. From top left: Longitudinal rolls (LR), varicose pattern (VP), subharmonic resonances (SR), periodically spaced kink lines (KL), undulations (UN) and transverse bursts (TB). Movies depicting dynamics of UN and TB are presented in [22].

For $28° < \theta < 72°$, a rather large region of slowly upward-drifting uniform undulations (UN) was observed. Here the bifurcation was characterized by a wave vector $\mathbf{q_1}$ with $s \cong 1.1 q_f$ and $\alpha \cong 20°$. In contrast, the corresponding instability observed in the unforced case sets in at considerably smaller θ and ε [dashed curve in Fig. 2(a)], and is of modulational type. Furthermore, without forcing, these patterns are defect turbulent [13]. This is an excellent demonstration of the stabilizing effect of forcing on spatiotemporal chaos. The UN became unstable, for higher

values of ε, to spatiotemporal chaos in the form of crawling rolls (CR), which were also found in the same parameter regime in the unforced system [12].

We now turn to the high inclination angles for which the dominant instability is shear induced. For $72° < \theta < 80°$, transverse bursts (TB) are observed. These were also found in the unforced cell, but only in a narrow range of angles in the immediate vicinity of θ_{cd}, in agreement with prior measurements [12]. For $80° < \theta < 90°$, as in the nonforced case for $\theta > \theta_{cd}$, a transverse roll state (TR) emerged at $\varepsilon \approx 0$ and longitudinal bursts (LB) were observed for higher values of ε.

Orthogonal forcing.—Figure 3(a) depicts the phase diagram for the orthogonal case, where transverse rolls (TR) were forced and prevailed at small ε while the competing LR were preferred at larger ε. None of the states observed immediately above the instability line of the TR was observed in the parallel case presented in Fig. 2(a), and the morphology of the phase diagram is completely different. At $\theta = 0$, a varicose pattern (VP) was observed, as in the parallel case. In the low inclination regime $0° < \theta < 10°$, a transition was observed to a stationary rhombic pattern [RO in Fig. 3(b)], which is spanned by wave vectors $\boldsymbol{q}_0 = (0, q_f)$ and $\boldsymbol{q}_1 = s[\cos(\alpha), \sin(\alpha)]$ with $s \cong 0.9 q_f$ and $\alpha \cong 10°$. We then observed, for $10° < \theta < 30°$, a bifurcation to an intriguing, stationary hexagonal structure. This state is spanned by three wave vectors $\boldsymbol{q}_0$, $\boldsymbol{q}_1$, and $\tilde{\boldsymbol{q}}_1$, where $q_1 \approx \tilde{q}_1 \approx q_c$. Here, in contrast to RO, both oblique modes ($\boldsymbol{q}_1$ and its symmetrical counterpart $\tilde{\boldsymbol{q}}_1$) participated in the destabilization, and together with the forcing mode fulfilled the resonant triad condition $\boldsymbol{q}_0 + \boldsymbol{q}_1 + \tilde{\boldsymbol{q}}_1 = 0$. We term this state hexarolls (HR) in analogy with a similar pattern found in centrifugally driven convection [19]. With increasing θ, the shear flow became more prevalent and enhanced the tendency to LR. Thus, in the following large interval of inclination angles, $30° < \theta < 75°$, the TR bifurcated to a bimodal (BM) state, characterized by a square structure spanned by TR and LR with wave number q_f. Note, however, that the wave number is locked, since the constituent LR are characterized by a wave number $q = q_f$, instead of $q = q_c^L$ in the absence of forcing. Bimodal patterns were observed in the nonforced cell only in the vicinity $\theta = \theta_{cd}$, where the buoyancy driven (LR) and shear flow driven (TR) destabilization mechanism become comparable near $\varepsilon = 0$. Transverse forcing considerably extends the BM region to lower inclination angles. The steep-angle interval, $75° < \theta < 90°$, was dominated by intriguing "heart" patterns (HP) arranged on a square lattice, which is aligned at 45° to the forcing orientation.

Over the whole range of θ and for higher ε, where the forcing influence is expected to diminish, secondary bifurcations were observed. The hexarolls were unstable to the chaotic state of crawling rolls, which have been introduced in the parallel forcing case. Quite interesting are the dynamic "scepter" patterns (SP). Here, extended subunits repeat periodically on a rectangular lattice, with a vertical

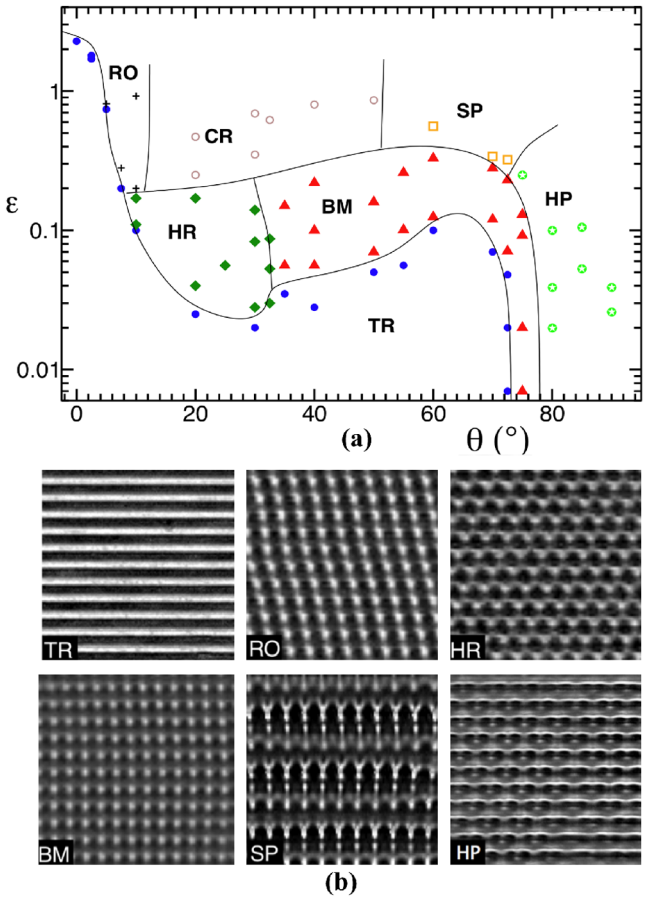

FIG. 3 (color online). Orthogonal Forcing. (a) Phase diagram. (b) Selected patterns (size of area shown as in Fig. 2): transverse rolls (TR), rhombic pattern (RO), hexarolls (HR), bimodals (BM), scepter-shaped patterns (SP), and heart-shaped patterns (HP). Movies depicting dynamics of BM, SP, and HP are presented in [22].

"superlattice" wave vector $q \cong q_f/2$. Recall that in the absence of forcing, one observes, at about the same ε and θ, chaotic transverse bursts (TB), characterized by the same subharmonic wave number. One could thus interpret SP as bursts stabilized by transverse forcing.

Weakly nonlinear convection.—In the following, we concentrate on a quantitative investigation of the amplitude of forced longitudinal rolls for small ε. We show it compares well with weakly nonlinear theory, essentially for the whole buoyancy dominated range.

In line with [17], the ε dependence of the amplitudes at small corrugation heights ($h \ll d$) can be described by mapping the surface corrugations to a temperature modulation of the bottom plate. The latter leads to a generic analytical expression for the temperature amplitude:

$$(\varepsilon + \varepsilon_0)A - g_0(q_f, \mathrm{Pr})A^3 + g_2(q_f)\delta = 0; \qquad (1)$$

here, the coefficients g_0 and g_2 are determined by theory [9] and δ was defined previously. The offset ε_0 originates from an increase of the critical temperature difference since $q_f \neq q_c$ and from a local increase in temperature

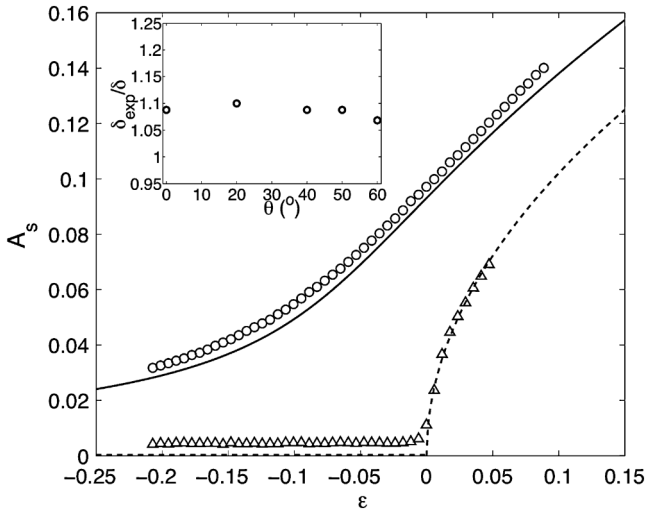

FIG. 4. (a) Bifurcation curve for parallel forcing at $\theta = 20°$. The triangles and circles represent the unforced and forced experimental data, respectively. The broken line represents the fitted square-root law of the unforced cell, and the solid line depicts the theoretical imperfect bifurcation curve. Small frame shows dependency of constant term (scaled by theoretical value) on inclination angle.

gradient due to corrugations. This experiment was done with a cell height $d = (520 \pm 2)\,\mu m$, yielding $q_f = 1.05 q_c^L$, $\delta = 0.025$, and $\varepsilon_0 = 0.009$.

The amplitude in (1) is related to the observed shadowgraph amplitude through the following expression [20]:

$$A_s = G(q_f/q_c)^2\left(c(q_f)\frac{\Delta T}{\Delta T_c(\theta)}\delta + A\right), \qquad (2)$$

where G depends on the shadowgraph setting and was extracted by fitting the data from the unforced cell, while the coefficient c was determined by theory [20].

As a representative example, we compare in Fig. 4 the Fourier coefficient $|A_0(\boldsymbol{q}_c)| \propto \sqrt{\varepsilon}$ for our unforced (small) cell with the corresponding one, $|A_s(\boldsymbol{q}_f)|$, of the forced cell, for $\theta = 20°$. The figure shows clearly the signature of an imperfect bifurcation near $\varepsilon = 0$ in the latter case. With increasing ε, the impact of forcing decreases and the curves of $|A_0|$ and $|A_s|$ approach each other.

The average values obtained from fitting the bifurcation data for inclination angles from $\theta = 0°$ up to $\theta = 60°$ (in order to avoid the regime effected by shear induced instabilities) are: $\langle \varepsilon_0 \rangle_{\text{exp}} = 0.03 \pm 0.01$, $\langle \delta \rangle_{\text{exp}} = 0.027 \pm 0.001$. The good agreement between the latter and the theoretical value is encouraging. This verifies that a small-amplitude surface corrugation can in general be mapped to a temperature modulation of the bottom plate. As expected, the description of longitudinal rolls via (1) works for the entire range investigated practically with the same parameters. This is demonstrated in the insert of Fig. 4, where we show δ_{exp} as function of θ.

In the present work, we have used inclined layer convection as a convenient system to study the combined effect of different externally imposed symmetry-breaking mechanisms. The relative weight of anisotropy due to inclination and forcing in the form of surface corrugations is tuned through the inclination angle θ and relative orientation angle φ. When the preferred orientations are parallel, the two mechanisms cooperate and stabilization of spatiotemporal chaos is observed. However, when the orientations are orthogonal, competing effects lead to spatial resonances, which are reflected in a variety of intriguing novel states such as "heart" and "scepter" patterns.

We gratefully acknowledge support from the Max Planck society and NSF under Grant No. DMR-0072077.

*eberhard.bodenschatz@ds.mpg.de

[1] W. B. Arthur, S. Durlauf, and D. A. Lane, *The Economy as an Evolving Complex System II* (Addison-Wesley, Reading, MA, 1997).
[2] F. Wolf and T. Geisel, Nature (London) **395**, 73 (1998).
[3] M. C. Cross and P. C. Hohenberg, Rev. Mod. Phys. **65**, 851 (1993).
[4] W. Tian and D. J. Parker, Mon. Weather Rev. **131**, 222 (2003).
[5] M. Kücken and A. C. Newell, J. Theor. Biol. **235**, 71 (2005).
[6] F. H. Busse and J. A. Whitehead, J. Fluid Mech. **47**, 305 (1971).
[7] D. Semwogerere and M. F. Schatz, Phys. Rev. Lett. **88**, 054501 (2002).
[8] M. Lowe and J. P. Gollub, Phys. Rev. A **31**, 3893 (1985).
[9] J. H. McCoy, Ph.D. thesis, Cornell University, 2007.
[10] A. Ogawa, W. Zimmermann, K. Kawasaki, and T. Kawakatsu, J. Phys. II (France) **6**, 305 (1996).
[11] V. H. Kurzweg, J. Heat Transfer **92**, 190 (1970).
[12] K. Daniels, B. Plapp, and E. Bodenschatz, Phys. Rev. Lett. **84**, 5320 (2000).
[13] K. Daniels and E. Bodenschatz, Phys. Rev. Lett. **88**, 034501 (2002).
[14] K. Daniels, O. Brausch, W. Pesch, and E. Bodenschatz, J. Fluid Mech. **597**, 261 (2008).
[15] J. R. de Bruyn *et al.*, Rev. Sci. Instrum. **67**, 2043 (1996).
[16] J. E. Hart, J. Fluid Mech. **47**, 547 (1971).
[17] R. E. Kelly and D. Pal, J. Fluid Mech. **86**, 433 (1978).
[18] P. Coullet and P. Huerre, Physica D (Amsterdam) **23**, 27 (1986).
[19] M. Auer, F. H. Busse, and R. M. Clever, J. Fluid Mech. **301**, 371 (1995).
[20] A_s is determined near $\varepsilon = 0$ by the vertical average of the temperature field $T(x, z)$ [21]. In addition to the main contribution ($\sim A$) fulfilling the amplitude Eq. (1), a small explicit correction should be taken into consideration, which contributes about 10% to A_s. This contribution is captured by $c(q_f)$. Details will be given elsewhere.
[21] S. P. Trainoff and D. S. Cannell, Phys. Fluids **14**, 1340 (2002).
[22] See EPAPS Document No. E-PRLTAO-101-088846 for video clips presenting the dynamics of selected states. For more information on EPAPS, see http://www.aip.org/pubservs/epaps.html.